Endothelial CXCL12 regulates neovascularization during tissue repair and tumor progression

Authors

Zeshaan N. Maan, MD, MSc, MRCS[1], Michael S. Hu, MD, MPH, MS[1]†, Robert Rennert, MD[1]†, Janos A. Barrera, MD[1], Dominik Duscher, MD[1], Michael Januszyk, MD, PhD[1], Alexander Whittam, BA[1], Jagannath Padmanabhan PhD[1], Nicholas Vial, MD[1], Natalie Ho[1], Lauren H. Fischer, MD[1], Johannes Riegler, PhD[2], Joseph C. Wu, MD, PhD[2], Michael T. Longaker, MD, MBA[1], Geoffrey C. Gurtner, MD, FACS[1]*

†These authors contributed equally to this work.

Affiliations

[1]Department of Surgery, Division of Plastic and Reconstructive Surgery, Stanford University School of Medicine, Stanford, California, USA

[2]Stanford Cardiovascular Institute, Stanford University School of Medicine, Stanford, California, USA

Short Title: Endothelial cell CXCL12 regulates tissue repair

***Corresponding Author:**

Geoffrey C. Gurtner, MD, FACS
Professor and Associate Chairman of Surgery
Stanford University School of Medicine
Department of Surgery, Division of Plastic and Reconstructive Surgery
257 Campus Drive West, Hagey building GK-201
Stanford, CA 94305-5148
Phone: (650) 724 - 6672
Fax: (650) 724 - 9501
E-mail: ggurtner@stanford.edu

Abstract

CXC chemokine ligand 12 (CXCL12; stromal cell-derived factor 1 [SDF-1]), primarily known for its role in embryogenesis and hematopoiesis, has also been implicated in tumor biology and neovascularization. However, its specific role and mechanism of action remain poorly understood. We previously demonstrated that CXCL12 expression is Hypoxia-Inducible Factor (HIF)-1 responsive. Here we use a conditional CXCL12 knockout mouse to show that endothelial-specific deletion of CXCL12 (eKO) does not affect embryogenesis, but reduces the survival of ischemic tissue, altering tissue repair and tumor progression. Loss of vascular endothelial CXCL12 disrupts endothelial – fibroblast crosstalk necessary for stromal growth and vascularization. Single-cell gene expression analysis in combination with a parabiosis model reveals a specific population of non-inflammatory circulating cells, defined by genes regulating neovascularization, which is recruited by endothelial CXCL12. These findings indicate an essential role for endothelial CXCL12 expression during the adult neovascular response in tissue injury and tumor progression.

Introduction

Adult neovascularization (new blood vessel growth in response to ischemia) plays a crucial role in tissue repair and regeneration and influences functional outcomes after injury to the heart, brain, and periphery . The complex biological processes governing neovascularization and tissue repair are exploited by tumor cells (Carmeliet et al., 2011; Hanahan et al., 2011), which typically exist in a setting of relative ischemia (Helmlinger et al., 1997). It is increasingly apparent that tumor survival and progression critically relies on the stromal microenvironment (Li et al., 2003). While numerous studies have explored the importance of a vascularized stroma to both physiologic tissue repair and pathologic tumor development (Valkenburg et al., 2018), an insufficient understanding of the underlying molecular mechanisms has limited the development of effective therapeutics to target this process.

Our laboratory and others have previously described the pivotal role of Chemokine (C-X-C motif) ligand 12 (CXCL12) in the recruitment of circulating cells to hypoxic tissue, secondary to stabilization of Hypoxia-Inducible Factor (HIF)-1 (Ceradini et al., n.d.), and regulation of stem cell microenvironments (Ding et al., 2013; Greenbaum et al., 2013). Interestingly, CXCL12 is also widely expressed in a number of human tumors and has a role in tumor progression and survival (Feig et al., 2013; Orimo et al., 2005; Teicher et al., 2010). These reports suggest a critical role for CXCL12 in both tissue repair and tumor progression, two physiological processes that depend on a delicate orchestration of molecular and cellular factors that govern neovascularization. The mechanisms underlying the influence of CXCL12 on these seemingly disparate processes remains unknown. We hypothesized that interrogating the role of CXCL12 in neovascularization would provide an opportunity to unravel the complex molecular mechanisms that underlie these processes.

Here we use a conditional CXCL12 knockout mouse to identify a critical role for vascular endothelial specific CXCL12 expression in neovascularization and tumor progression. Knockout of endothelial-specific CXCL12 inhibits wound healing and ischemic tissue survival. Surprisingly, loss of endothelial CXCL12 expression completely abrogates tumor growth despite high levels of continued CXCL12 expression by both tumor cells and tumor-associated fibroblasts. We demonstrate that loss of endothelial CXCL12 inhibits fibroblast proliferation, survival, and expression of angiogenic cytokines, clarifying the importance of endothelial-fibroblast cross-talk in this process. Finally, utilizing single-cell gene expression analyses in combination with a parabiosis model, we identify a non-inflammatory progenitor cell subpopulation exclusively recruited to tissue by endothelial CXCL12 signaling. These data reveal a crucial role for vascular endothelial-derived CXCL12 in both tissue repair and tumor progression and uncover a paracrine mechanism governing the formation of vascularized stroma.

Results

Vascular endothelial derived CXCL12 does not regulate embryogenesis or vasculogenesis

To specifically assess the role of endothelial CXCL12 during neovascularization, we engineered a floxed allele of *Cxcl12* (*Cxcl12* $^{loxP/loxP}$) (Figure 1A). *Rosa-creER* and *Tie2-cre* transgenes were utilized to generate tamoxifen-inducible global CXCL12 knockout (gKO) and endothelial-cell-specific (Ding et al., 2013; Greenbaum et al., 2013; Kisanuki et al., 2001) CXCL12 knockout (eKO) mice (Figure 1B), respectively. CXCL12 knockout progeny (*CXCL12*$^{loxP/loxP}$; *ROSA-creER*$^{+/-}$, *Tie2-cre* $^{+/-}$) were viable, fertile, produced at expected Mendelian ratios and showed no overt pathologic phenotype. We confirmed DNA recombination upon tamoxifen administration with a subsequent >80% decrease in mRNA and protein expression of CXCL12 (Figure 1C-E). Endothelial specific knockout of CXCL12 was additionally validated used immunostaining (Figure 1F). Prior work has demonstrated that stromal expression of CXCL12 is critical during embryogenesis (Nagasawa et al., 1996), cardiac development (Nagasawa et al., 1996; Tachibana et al., 1998), hematopoiesis (Nagasawa et al., 1996), and organ vascularization (Tachibana et al., 1998). Immunostaining and standard histology were utilized to examine organ development and vascularization in eKO mice and demonstrated normal morphology and vascular pattern (Supplementary Figure 1). This suggests that endothelial CXCL12 does not have a primary role during organogenesis and vascular development.

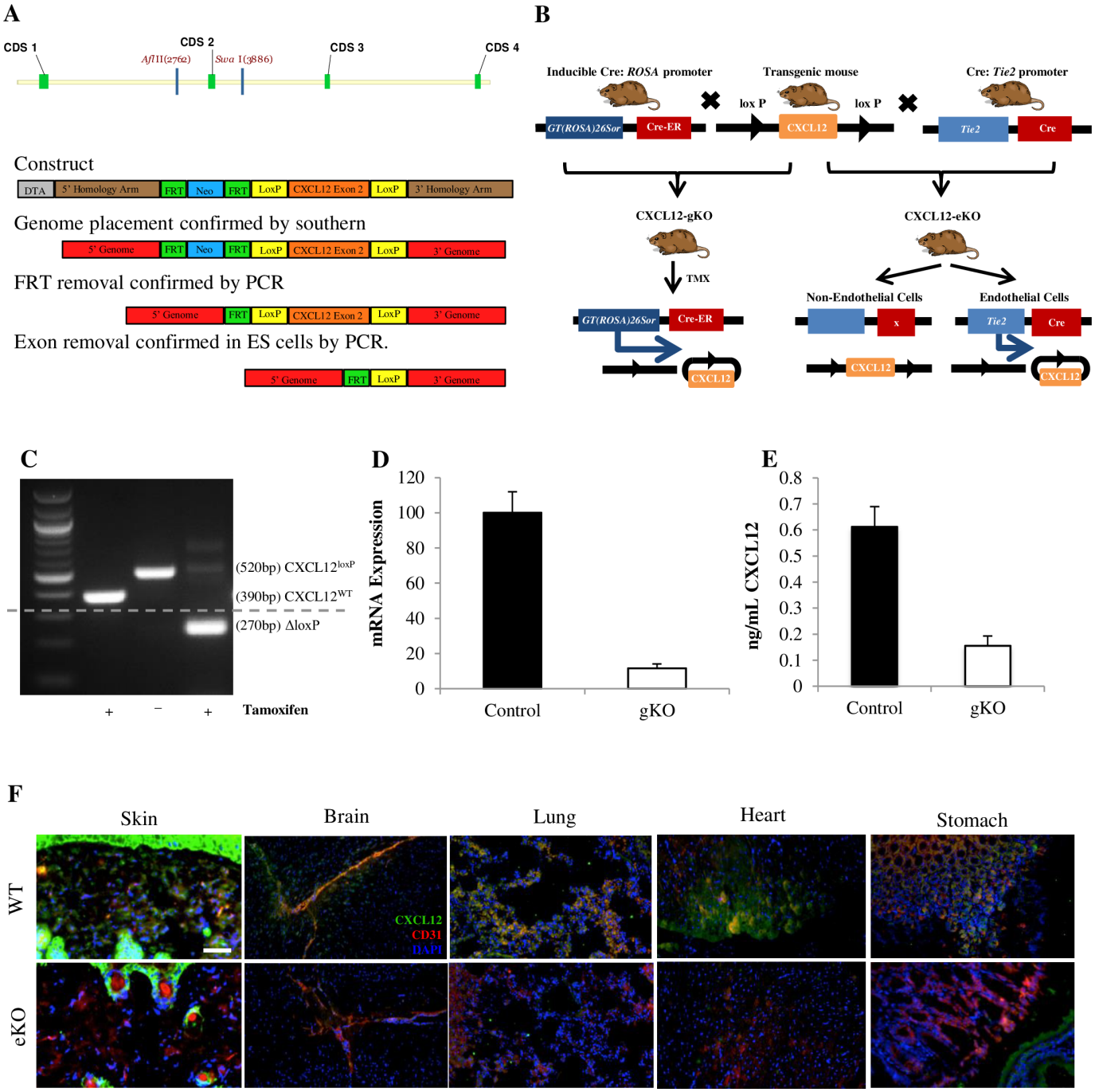

Figure 1. Development and validation of gKO and eKO CXCL12 mice.

(A) Schematic of the murine Cxcl12 locus depicting our approach to homologous recombination in embryonic stem cells to generate a floxed Cxcl12 allele. Cxcl12 floxed mice were crossed with mice carrying the *Cre-recombinase* transgene to generate tissue-specific knockout progeny) (B) Schematic of the breeding strategy used to generate tamoxifen inducible global Cxcl12 knockout (gKO) and endothelial-cell specific Cxcl12 knockout (eKO) mice. (C) PCR validation of the presence and recombination of the floxed allele upon exposure of gKO mice to tamoxifen. (D) qRT-PCR of Cxcl12 expression in the skin of tamoxifen induced gKO mice compared to control. (E) ELISA for Cxcl12 levels in the skin of tamoxifen induced gKO mice compared to control. (F) Immunohistochemical analysis showing overlapping expression of CXCL12 and CD31 in wild type but not eKO mice. Images obtained with a Zeiss Axioplan 2 fluorescence microscope, magnification x20, scale bar 200 μm.

Vascular endothelial CXCL12 critically regulates neovascularization and tissue repair.

We then investigated the role of CXCL12 in adult tissue repair using an excisional cutaneous injury model in eKO and gKO mice (Galiano et al., 2004). We found that both eKO and gKO mice showed delayed healing of their wounds compared to floxed control mice (16 days vs. 11 days, respectively) (Figure 2A, B). The impairment in tissue repair in both knockout groups was apparent by the 4th day after injury, as measured by remaining wounded area (Figure 2C). The similar healing times of eKO and gKO mice (Figure 2A-C) suggests that endothelial cells are the critical source of CXCL12 during the repair of injured tissue in adults. Microscopically, the most obvious difference in the healed tissue of eKO mice was a decreased vascular density by immunostaining (Figure 2D, E). We analyzed the injured tissue at earlier time points and found reduced transcription and protein expression of CXCL12 in eKO mice. In addition, VEGF and FGF-2 transcription and protein expression were diminished (Figure 2F-H), suggesting that the CXCL12 signaling modulates other HIF-1 regulated, angiogenic signaling pathways. To confirm the critical role of endothelial CXCL12 signaling during neovascularization, we used a dorsal ischemic skin flap model (Ceradini et al., n.d.), which demonstrated decreased tissue survival in eKO versus wild type mice (Figure 3A-D). Similarly, using a myocardial ischemia model (Patten et al., 1998), in which the left coronary artery is ligated, there was decreased myocardial vessel density in eKO mice (Figure 3E,F).

147

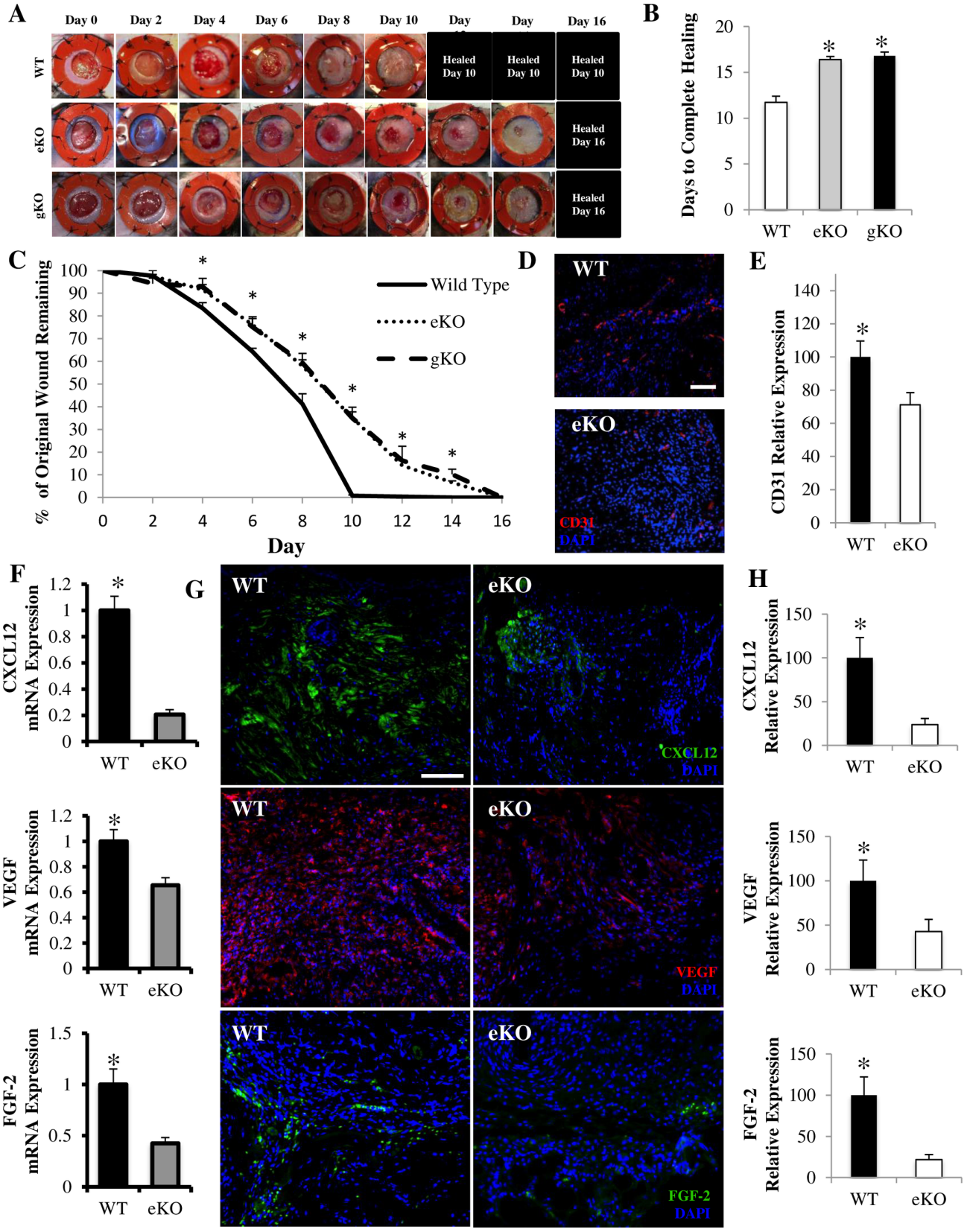

Figure 2. Wound healing relies on endothelial CXCL12.

(A) Representative images of similarly delayed healing in endothelial specific (eKO) and global CXCL12 knockout (gKO) mice compared to wild type (WT). (B, C) Both eKO and gKO mice require 16 days to heal compared to 11 days in control. (D, E) Decreased vascular density in fully healed wounds of eKO mice. Images obtained with a Zeiss Axioplan 2 fluorescence microscope, magnification x20, scale bar 200 µm. (F) Decreased expression of Ccxl12 (top), Vegf (middle), and Fgf2 (bottom) in the wounds of eKO mice. (G, H) Selective loss of CXCL12 (top) and decreased levels of VEGF (middle) and FGF-2 (bottom) in eKO mice. Magnification x20, scale bar 200 µm.

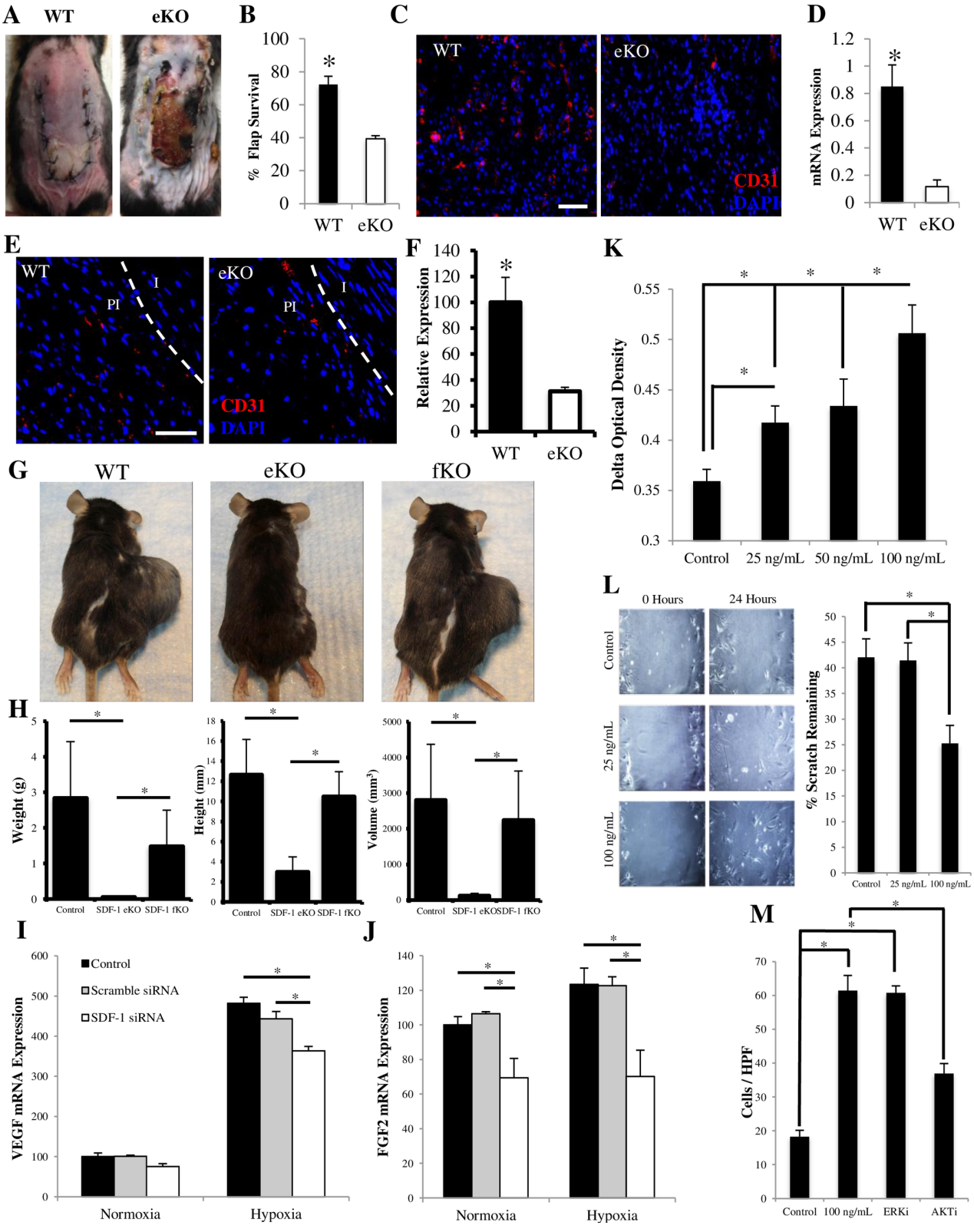

Figure 3. Endothelial CXCL12 regulates neovascularization, stroma formation, and tumor progression.

(A, B) Decreased ischemic skin flap survival in eKO mice. (C, D) Decreased vascular density in ischemic tissue of eKO mice. Images obtained with a Zeiss Axioplan 2 fluorescence microscope, magnification x20, scale bar 200 μm. (E, F) Decreased vascular density in peri-infarct zone of eKO myocardium. (PI = peri-infarct zone; I = infarct zone). Magnification x20, scale bar 200 μm. (G, H) Significantly reduced tumor burden in eKO mice. (fKO = fibroblast specific CXCL12 knockout) (I, J) Decreased fibroblast expression of VEGF and FGF-2 in the presence of decreased endothelial expression of CXCL12. (K, L, M) Increased fibroblast proliferation, migratory capacity, and survival (mediated by PI3K/AKT signaling) in response to CXCL12. Images obtained with a Zeiss Axioplan 2 fluorescence microscope, magnification x20, scale bar 200 μm.

Tumor growth is dependent on host vascular endothelial CXCL12 expression

Cancer cells, which typically exist in the setting of relative ischemia (Helmlinger et al., 1997) appear to rely on the stromal microenvironment for tumor growth, angiogenesis, and invasion (Li et al., 2003). In particular, melanoma has been shown to rely on its surrounding stroma (Flach et al., 2011) and CXCL12, typically derived from cancer cells, has been implicated in tumor progression and survival (Teicher et al., 2010), including in B16 murine melanoma cells (Mendt et al., 2017). To determine if host endothelial CXCL12 had a role in tumor stroma formation and tumor progression, we transplanted B16 murine melanoma cells into control, eKO, and fibroblast-specific (*Col1a2-creER* transgene) (Ubil et al., 2014; Zheng et al., 2002) CXCL12 knockout (fKO) mice. The fKO model was chosen in order to study whether stromal cells themselves produce CXCL12 in sufficient amounts to drive tumor progression, independent of endothelial cell or other circulatory sources. Tumor measurements demonstrated completely abrogated tumor growth only in eKO mice (Figure 3G, H), suggesting a pivotal role for host endothelial CXCL12 in tumor progression.

Vascular endothelial CXCL12 regulates fibroblast gene expression, proliferation and migration

The establishment of new vascularized tissue, or stroma, requires a coordinated interplay between endothelial cells and fibroblasts (Fukumura et al., 1998; Newman et al., 2011; Stratman et al., 2009). To explore the role of CXCL12 in endothelial – fibroblast cross talk, we used siRNA to target CXCL12 in human microvascular endothelial cells co-cultured with normal human dermal fibroblasts. Decreasing endothelial production of CXCL12 reduced fibroblast expression of VEGF and FGF-2 in response to hypoxia (Figure 3I, J). These data suggest that hypoxia-responsive fibroblast expression of VEGF and FGF-2, which stimulate endothelial cells to proliferate and form new vessels, is in turn reliant on vascular endothelial expression of CXCL12 and provide a possible mechanism for our earlier immunostaining

results in injured eKO skin (Figure 2F-H). Additionally, VEGF has been shown to impart drug resistance to tumor endothelial cells within the tumor stroma (Hida et al., 2013), which suggests that endothelial CXCL12 may induce drug resistance in tumors through a paracrine mechanism. Next, we treated fibroblasts with recombinant CXCL12 and demonstrated increased proliferation and migratory capacity (Figure 3K, L). CXCL12 also enhanced the survival of fibroblasts in a low nutrient environment (Figure 3M). It has become increasingly evident that the tumor microenvironment plays a critical role in cancer progression and treatment outcomes. Collectively, these data reveal a novel mechanism by which host endothelial CXCL12 governs the formation of a critical component of this microenvironment and, therefore, tumor progression.

Vascular endothelial CXCL12 recruits a unique non-inflammatory circulating cell to injured tissue

Because the endothelium is the primary interface between the circulation and the tissue it supplies, and as endothelial cells are crucial for inflammatory cell recruitment (Lawrence et al., 1991; Möhle et al., 1998), we asked whether endothelial specific CXCL12 has a role in the recruitment of non-inflammatory circulating cells that may participate in the neovascularization of hypoxic tissue. Wild type and eKO recipient mice were parabiosed to GFP positive donor mice and cross-circulation was confirmed after 3 weeks using fluorescent imaging and FACS analysis (Figure 4A). Excisional wounds were subsequently created on the dorsum of eKO recipient mice and demonstrated reduced recruitment of mature hematopoietic lineage negative (Ly6C/G, CD45R, TER119, CD4, CD8, and CD11b), GFP positive cells (Figure 4B,C), which would include all types of progenitor cells and exclude inflammatory cells such as neutrophils and lymphocytes. To better characterize the progenitor cells differentially recruited to eKO and control recipient mice, we utilized microfluidic technology to apply a massively parallel single cell transcriptional analysis (SCA) (Supplementary Figure 2, Supplementary Figure 3). Partitional clustering

218 revealed four transcriptionally distinct subpopulations of non-inflammatory progenitor cells in injured
219 tissue. One of these subpopulations (cluster 2) was completely absent in eKO mice, while another was
220 reduced in eKO mice. The remaining two populations were preserved across control and eKO mice (Figure
221 4D, Supplementary Figure 4, Supplementary Figure 5). The subpopulation completely absent from injured
222 eKO tissue was defined by increased expression of genes associated with progenitor cells, such as Ckit
223 and Mcam, and vascular genes, such as Pecam1, Flt1, Tie1, and Tek. Additionally, this population
224 differentially expressed the cellular adhesion gene Itgb3 (Figure 4E). Pathway analysis software was used
225 to generate a transcriptional network utilizing those genes differentially expressed in this cluster as seed
226 genes. "Inferred" genes included those known to be implicated in cell survival (Erk1/2, Akt, Nfkb
227 complex), neovascularization (Vegf, Pdgfb), and extracellular matrix interactions (Fak). The overall
228 associated biological functions of this network included Cardiovascular System Development and
229 Function, Cellular Movement, and Cell Morphology (Figure 4F). Collectively, these data indicate that
230 endothelial CXCL12 signaling regulates the recruitment of a unique non-inflammatory circulating cell to
231 injured tissue.
232

233

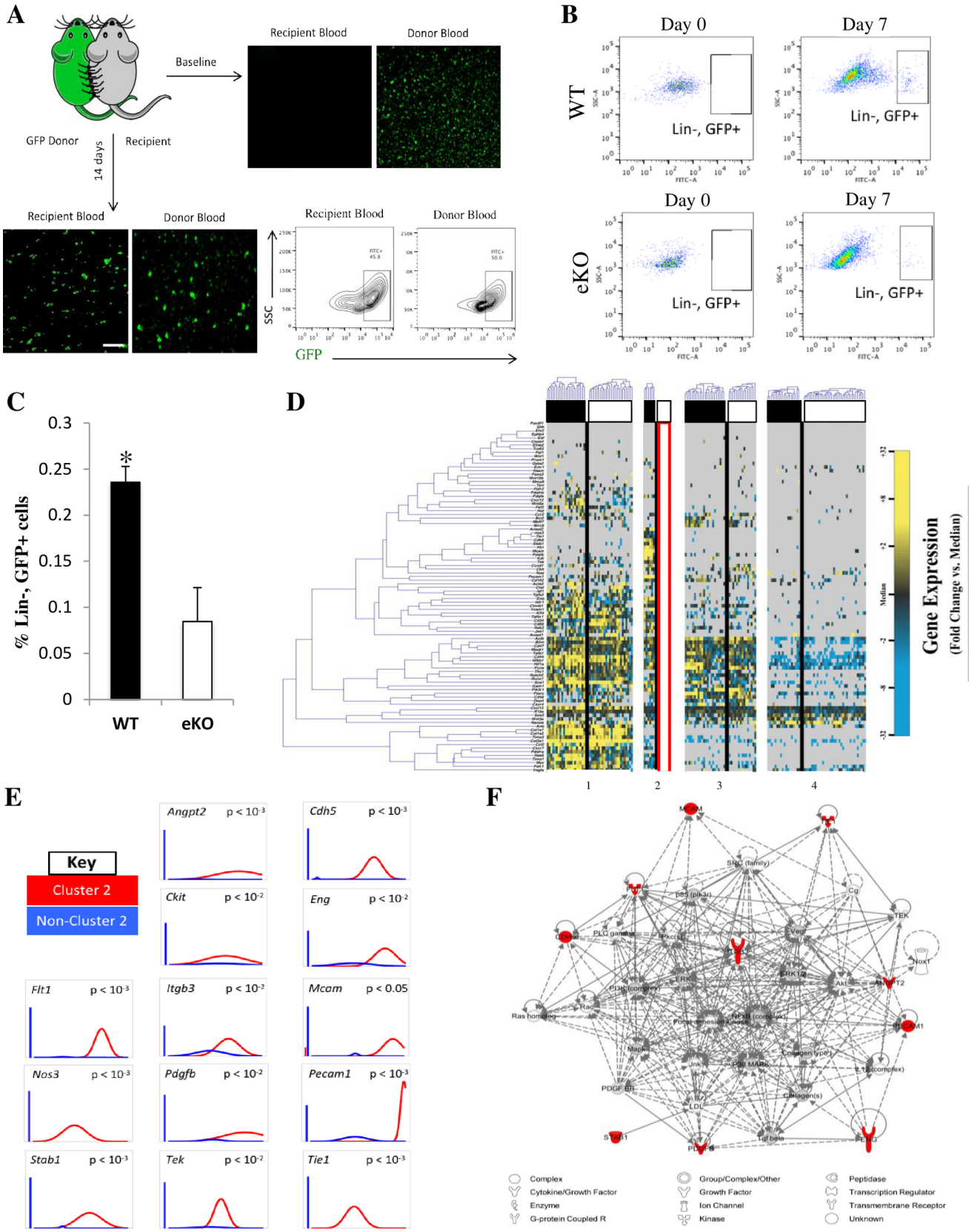

Figure 4. Endothelial CXCL12 regulates recruitment of progenitor cells in ischemic tissue.

(A) Parabiosis schema and demonstration of cross-circulation. Images obtained with a Zeiss Axioplan 2 fluorescence microscope, magnification x20, scale bar 200 μm. (B, C) Decreased recruitment of non-inflammatory circulating cells to wounds of eKO mice. (D) Single-cell analysis demonstrating absence of sub-population of non-inflammatory circulating cells from wounds of eKO mice. (E) Differentially expressed genes defining cell population absent from eKO wounds. Left bar for each panel represents fraction of cells that failed to amplify. (F) Top scoring Ingenuity Pathway Analysis (IPA)-constructed transcriptome network based on population defining "seed" genes (E). Seed genes are colored in red, inferred genes in grey.

Discussion

We describe the differential function of CXCL12 depending on its physiological context and tissue of origin: endothelial expression does not regulate organ development or vascularization during embryogenesis, in contrast to stromal CXCL12 expression (Tachibana et al., 1998), but it does influence the expression of hypoxia-responsive, angiogenic genes and regulates the neovascular response during both the repair of injured tissue and tumor progression. Although the chemotactic effect of CXCL12 in the context of leukocytes has been investigated (Campbell et al., 1998), its physiological function and cellular source in the context of injury had not been previously elucidated. We propose that a distinct population of circulating, non-inflammatory progenitor cells that originate from the bone marrow are exclusively trafficked to injured tissue by CXCL12 mediated angiocrine signaling.

Our findings extend previous work examining the relationship between tumor pathobiology and the mechanisms underlying tissue repair (tumor/wound). Targeting the tumor microenvironment is an emerging paradigm in the management of resistant tumors. Our results demonstrate that host CXCL12 critically regulates the microenvironment independent of tumor derived CXCL12, presenting a potential target for clinical therapy. However, it remains unclear why the selective inactivation of CXCL12 in endothelial cells has such profound effects on tumor growth despite expression of CXCL12 by several other cell types, including tumor endothelial cells. Our findings may also have implications for the development of personalized oncological therapies, as understanding patient-specific biological responses to cancer may be more crucial than tumor profiling. While this study does not exhaustively explore the mechanisms underlying the similar effects of endothelial CXCL12 on tumor growth and tissue repair, there is increasing evidence in the literature of the molecular and cellular similarities between wound

267 healing and tumorigenesis (Arwert et al., 2012; Flier et al., 1986; Schäfer et al., 2008). Further research
268 parsing out potential differences are likely necessary to inform the development of clinical therapies.

Materials and Methods

Mice

All transgenic strains had been backcrossed at least ten generations onto a C57BL/6 background (Jackson Laboratories, Bar Harbor, ME). *Rosa–creER*, *Tie2–cre(14)* and *Col1a2-creER* mice were obtained from the Jackson Laboratory. GFP positive *C57BL/6-Tg(CAG-EGFP)1Osb/J* mice were similarly obtained from Jackson Laboratory. Mice were maintained under standard pathogen-free conditions according to methods approved by the Stanford University Administrative Panel on Laboratory Animal Care (APLAC). All animal experiments were compliant with ethical regulations and approved by the Stanford University APLAC.

Generation of CXCL12$^{loxP/loxP}$ Mice

A floxed allele of *Cxcl12* was generated by inserting *LoxP* sites flanking exon 2 of *Cxcl12*. FRT sites were inserted flanking the neomycin selection cassette (Figure 1). Generation of targeted embryonic stem cells and blastocyst injections were performed as previously described (Greenbaum et al., 2013). Excision of the neomycin cassette was accomplished through FLP-FRT recombination. Mice were genotyped using PCR primers: *Cxcl12*^{loxP} forward, 5′-ACCCATAAATTGAAACATTTGG-3′; *Cxcl12*^{loxP} reverse, 5′-TTCTACCACCTGCAGTTTTCC-3′; *Cxcl12*^{loxP} recombined, 5′-GGTAAATTTATCGAATTCCGAA-3′.

Animal Studies

Animal studies were performed with n=5 animals, and repeated at least twice, unless otherwise specified. Mice were 12-16 weeks of age at start of experiments.

Murine Excisional Wound Model

Splinted excisional wounds were created as previously described (Galiano et al., 2004). Briefly, using a 6-mm biopsy punch (Integra Miltex, Plainsboro, NJ), two 6-mm full thickness wounds were created on the shaved dorsum of anesthetized mice. In parabiotic pairs, the recipient mouse was only wounded on the non-parabiosed side. A donut-shaped silicone splint (10-mm diameter) was centered on the wound and secured to the skin using an immediate-bonding adhesive (Krazy Glue; Elmer's Inc., Columbus, Ohio) and 6-0 nylon sutures (Ethicon Inc. Somerville, NJ) to prevent wound contraction. All wounds were covered using an occlusive dressing (Tegaderm; 3M, St. Paul, MN). Following surgery, the mice were placed on warming pads and allowed to fully recover from anesthesia before being returned to the institutional animal facility. Digital photographs were taken at regular intervals and wound area was measured using ImageJ software (NIH) (n = 6 mice). All measurements were performed by a blinded observer. Wound tissue was harvested on post-wounding day 7 and once wounds were completely healed using an 8mm punch biopsy.

Murine Ischemic Skin Flap Model

A reproducible model of graded soft tissue ischemia was created on the dorsum of mice as previously described (Valkenburg et al., 2018). Briefly, a full thickness (epidermis, dermis, and underlying adipose tissue) 3-sided peninsular flap (1.25 x 2.5 cm) was created on the shaved dorsum. The flap was elevated from the underlying muscular bed and a 0.13 mm thick silicone sheet was inserted to separate the skin from the underlying tissue. The skin flap was sutured back into place with 6-0 nylon sutures. This model creates a gradient of increasing ischemia from proximal to distal. Digital photographs were taken at regular intervals and necrosed area was measured using ImageJ software (NIH) (n = 6 mice). All measurements were performed by a blinded observer.

316 *Murine Myocardial Infarction Model*

317 Ligation of the mid left anterior descending (LAD) artery was performed by a single experienced surgeon
318 (JR) as previously described (Patten et al., 1998). Infarction was confirmed by myocardial blanching and
319 EKG changes. Animals were euthanized and hearts explanted at postoperative day 30 (n=6 mice, repeated
320 once).

321

322 *Murine Parabiosis Model*

323 GFP positive "donor" and either control or eKO "recipient" mice were shaved and anesthetized. Parabiosis
324 surgery was performed as previously described (n=5 mice analyzed) (Bunster et al., 1933; Wagers et al.,
325 2002). Briefly, the corresponding flanks of mice were shaved and disinfected with betadine solution and
326 70% ethanol. Matching skin incisions were made from the olecranon to the knee joint of each mouse. The
327 skin edges were undermined to create about 1 cm of free skin. 6-0 nylon sutures were used to approximate
328 the dorsal and ventral skin. The skin was over-sewn to protect the suture line. Mice were allowed to
329 recover as described above. Buprenorphine was used for analgesia by subcutaneous injection every 8–12
330 hours for 48 hours post operation. After three weeks, cross-circulation was confirmed using fluorescent
331 microscopy and FACS analysis (Figure 4A).

332

333 *Murine Tumor Model*

334 A 1 cm incision was created on the right flank of shaved and anesthetized control, eKO, and fKO mice. A
335 1x1 cm subcutaneous pocket was created and a hydrogel (Wong et al., 2010) seeded with 2.5 x 10^5 B16-
336 F10 melanoma cells (ATCC CRL-6475) was implanted and the incision closed with 6-0 nylon suture.
337 Measurements for length, width, and height were taken with a digital caliper and tumor volume was
338 calculated using the formula: V = 0.5 x (L x W x H), where V is tumor volume, L is length, W is width,

and H is height. Tumor sizes were measured by the same, blinded observer every other day until mice were euthanized at 4 weeks.

Blood and Skin Analysis

Mononuclear cells from blood were obtained from the buffy coat layer following Ficol-Paque density centrifugation (Jaatinen et al., 2007). Skin samples, including wounded tissue and ischemic skin, were digested and cells isolated as previously described (Suga et al., 2014).

Histology and Tissue Analysis

For fixation, tissues were placed in 2% paraformaldehyde for 12-16 hours at 4ºC. Samples were prepared for embedding by soaking in 30% sucrose in PBS at 4ºC for 24 hours. Samples were removed from the sucrose solution and tissue blocks were prepared by embedding in Tissue Tek O.C.T (Sakura Finetek) on dry ice. Frozen blocks were mounted on a MicroM HM550 cryostat (MICROM International GmbH) and 5-8 micron thick sections were transferred to Superfrost/Plus adhesive slides (Fisher & Company, Inc.).

Immunohistochemistry

For hematoxylin and eosin staining, standardized protocols were used with no modifications. Sections were visualized using Leica DM4000B microscope (Leica Microsystems). Immunostaining on frozen sections was performed using the following primary antibodies: CD31 (Abcam 28364), SDF-1 (Abcam 25117), VEGF (Abcam 52917), and FGF-2 (Abcam 8880). Briefly, slides were fixed in cold acetone (-20°C), and then blocked for 1 hour in 5% goat serum at room temperature followed by incubation with primary antibody for 12-16 hours at 4°C. Slides were then incubated for 1 hour with goat anti-rabbit Alexa Fluor 488 conjugate (Invitrogen A-11034) or 594 conjugate (Invitrogen A-11037). A Zeiss Axioplan 2

362 fluorescence microscope was used to image the slides (Carl Zeiss, Inc., Thornwood, NY). Quantification
363 of fluorescence was performed by a blinded observer using ImageJ software (NIH).
364
365 **Flow Cytometry**
366 All flow cytometry analysis was performed on dissociated wound tissue or blood. Cells were stained by
367 standard protocols with the following fluorescently conjugated antibodies (eBiosciences unless otherwise
368 noted). Lineage analysis was assessed using R-Phycoerythrin (PE)-Cy5-conjugated Ly6C/G (RB6-8C5,
369 Gr-1, myeloid), CD45R (RA3-6B2, B220, B lymphocytes), TER119, CD4, CD8, and CD11b. Cells not
370 stained with these antibodies were incubated with the proper isotype controls or left unstained. Cells were
371 resuspended in FACS buffer and DAPI prior to FACS analysis on a FACSAria II. At least 50,000 events
372 were recorded per sample. Data were analyzed using FlowJo digital fluorescence-activated cell sorting
373 software by a single blinded evaluator (Tree Star Inc, Ashland, OR).
374
375 **Quantitative Reverse-Transcription PCR**
376 RNA was isolated using an RNeasy Mini Kit (Qiagen, Hilden, Germany) according to the manufacturer's
377 instructions. Reverse transcription was performed with 500 ng RNA using the SuperScript III First-Strand
378 Synthesis System (Invitrogen, Carlsbad, CA). qRT-PCR was carried out using TaqMan® Assays-on-
379 Demand™ Gene Expression Products from Applied Biosystems (Foster City, CA, USA): Cxcl12, assay
380 ID Mm00445552_m1; Vegfα, assay ID Mm01281447_m1; Fgf2, assay ID Mm00433287_m1. mRNA
381 expression levels were normalized to B2m expression, assay ID Mm00437762_m1, and presented as
382 relative values.
383
384

In Vitro Assays

Human dermal fibroblasts (HdFbs) (Life Technologies C0135C) and human dermal microvascular endothelial cells (HdMVECs) (Life Technologies C01125PA) were purchased and used for *in vitro* assays. All assays were conducted in triplicate unless otherwise stated.

Co-Culture

Indirect co-culture experiments were performed using 6-well plates and 0.4 μM pore trans-well inserts. HdFb were seeded in the upper chamber and HdMVECs were seeded in the lower chamber. si-CXCL12 and scrambled-siRNA were purchased form Life Technologies. HMVECs were transfected using Lipofectamine RNAiMAX Reagent (Life Technologies) according to the manufacturer's protocol before co-culture with HdFb in normoxia and hypoxia as previously described (Ceradini et al., n.d.).

Proliferation

Human dermal fibroblasts were plated in 96-well cell-culture plates, 2500 cells/well, in 150 μL of medium with 1% FBS. After 24 hours, fresh media with 1% FBS alone or with varying concentrations of recombinant CXCL12 (25, 50, and 100 ng/mL) were added and after an additional 6 hours BrdU was added and a cell proliferation assay was performed according to the manufacturer's instructions (Roche Applied Sciences).

Migration

Scratch assay was performed as previously described (Wang et al., 2018) on HdFb cultured in 24-well plates with culture medium containing 1% FBS alone or with varying concentrations of recombinant CXCL12 (25 and 100 ng/mL).

Survival

HdFb were cultured until 90% confluent in 24-well plates. They were then placed in culture medium containing 1% FBS for 24 hours then cultured in medium containing 0.5% FBS alone, 100 ng/mL recombinant CXCL12, 100 ng/mL recombinant CXCL12 + U0126 (Cell Signaling Technology), or 100 ng/mL recombinant CXCL12 + LY294002 (Cell Signaling Technology). After 72 hours, images of 5 HPFs/well were captured and recorded under phase contrast microscopy and manual cell counts were performed by a blinded observer.

Microfluidic Single-Cell Gene Expression Analysis

Gene lists were collected from a literature search. Single cell reverse transcription and low cycle pre-amplification were performed as previously described (Glotzbach et al., 2011; Januszyk et al., 2014). Briefly, wound lysate cell suspensions were sorted from *Tie-2*^{Cre}*/CXCL12*$^{loxP/loxP}$ and *CXCL12*$^{loxP/loxP}$ transgenic mice as single progenitor cells into each well of a 96-well plate using a Becton Dickinson FACSAria flow cytometer (Franklin Lakes, NJ) into 6 µl of lysis buffer and SUPERase-In RNAse inhibitor (Applied Biosystems, Foster City, CA) (N=5 mice). Live/dead gating was performed based on DAPI exclusion. Progenitor cells were defined as previously described. Reverse transcription and low cycle pre-amplification were performed using Cells Direct (Invitrogen) with Taqman assay primer sets (Applied Biosystems) as per the manufacturers specifications. Exon-spanning primers were used where possible to avoid amplification of genomic background. cDNA was loaded onto 96.96 Dynamic Arrays (Fluidigm, South San Francisco, CA) for qPCR amplification using Universal PCR Master Mix (Applied Biosystems) with a uniquely compiled Taqman assay primer set (Supplementary Table 1) as previously described (Glotzbach et al., 2011).

Statistical Analysis

For comparison between two groups, students t-tests were used with a P-value < 0.05 considered statistically significant. Analysis of single cell data was performed as described previously (Glotzbach et al., 2011; Januszyk et al., 2014; Levi et al., 2011). Briefly, data from all samples were normalized relative to the pooled median expression for each gene and converted to base 2 logarithms. Absolute bounds (+/- 5 cycle thresholds from the median or 32-fold increases/decreases in expression) were set, and non-expressers were assigned to this floor. Clustergrams were then generated using hierarchical clustering (with a 'complete' linkage function and Euclidean distance metric) to facilitate data visualization (MATLAB R2011b, MathWorks, Natick, MA).

To detect overlapping patterns within the single cell transcriptional data, k-means clustering was employed using a standard Euclidean distance metric. Accordingly, each cell was assigned membership to a specific cluster as dictated by similarities in expression profiles (minimizing the within-cluster sum of square distances) in MATLAB. Optimally partitioned clusters were then sub-grouped using hierarchical clustering to facilitate visualization of data patterning (Fukumura et al., 1998; Newman et al., 2011). Non-parametric, two-sample Kolmogorov-Smirnov (K-S) tests were used to identify those genes with expression patterns that differed significantly between population clusters and/or groups, following Bonferroni correction for multiple samples using a strict cutoff of $p<0.05$. For subgroup comparisons, the empirical distribution of cells from each cluster was evaluated against that of the remaining cells in the experiment. Ingenuity Pathway Analysis (IPA, Ingenuity Systems, Redwood City, CA) was used to construct transcriptome networks based on genes that were significantly increased within clusters (including both direct and indirect relationships).

Data Sharing Statement

Original data may be obtained by e-mail request to the corresponding author. Single cell transcriptional data is available at GEO under accession number GSE146529.

Acknowledgments

We thank Theresa Carlomagno for administrative support and Yujin Park for help with tissue processing.

Competing interests: The authors declare no conflicts of interest.

References

Arwert, E. N., Hoste, E., & Watt, F. M. (2012). Epithelial stem cells, wound healing and cancer. *Nature Reviews. Cancer*, *12*(3), 170–180. doi: 10.1038/nrc3217

Brem, H., & Tomic-Canic, M. (2007). Cellular and molecular basis of wound healing in diabetes. *The Journal of Clinical Investigation*, *117*(5), 1219–1222. doi: 10.1172/JCI32169

Bunster, E., & Meyer, R. K. (1933). An improved method of parabiosis. *The Anatomical Record*, *57*(4), 339–343. doi: 10.1002/ar.1090570404

Campbell, J. J., Hedrick, J., Zlotnik, A., Siani, M. A., Thompson, D. A., & Butcher, E. C. (1998). Chemokines and the arrest of lymphocytes rolling under flow conditions. *Science (New York, N.Y.)*, *279*(5349), 381–384. doi: 10.1126/science.279.5349.381

Carmeliet, P., & Jain, R. K. (2011). Molecular mechanisms and clinical applications of angiogenesis. *Nature*, *473*(7347), 298–307. doi: 10.1038/nature10144

Ceradini, D. J., Kulkarni, A. R., Callaghan, M. J., Tepper, O. M., Bastidas, N., Kleinman, M. E., Capla, J. M., Galiano, R. D., Levine, J. P., & Gurtner, G. C. (n.d.). Progenitor cell trafficking is regulated by hypoxic gradients through HIF-1 induction of SDF-1. *Nature Medicine*, *10*(8), 858–864.

Chen, J., Zhang, Z. G., Li, Y., Wang, L., Xu, Y. X., Gautam, S. C., Lu, M., Zhu, Z., & Chopp, M. (2003). Intravenous administration of human bone marrow stromal cells induces angiogenesis in the ischemic boundary zone after stroke in rats. *Circulation Research*, *92*(6), 692–699. doi: 10.1161/01.RES.0000063425.51108.8D

Ding, L., & Morrison, S. J. (2013). Haematopoietic stem cells and early lymphoid progenitors occupy distinct bone marrow niches. *Nature*, *495*(7440), 231–235. doi: 10.1038/nature11885

492 Feig, C., Jones, J. O., Kraman, M., Wells, R. J. B., Deonarine, A., Chan, D. S., Connell, C. M., Roberts,
493 E. W., Zhao, Q., Caballero, O. L., Teichmann, S. A., Janowitz, T., Jodrell, D. I., Tuveson, D. A.,
494 & Fearon, D. T. (2013). Targeting CXCL12 from FAP-expressing carcinoma-associated
495 fibroblasts synergizes with anti-PD-L1 immunotherapy in pancreatic cancer. *Proceedings of the*
496 *National Academy of Sciences of the United States of America*, *110*(50), 20212–20217. doi:
497 10.1073/pnas.1320318110
498 Flach, E. H., Rebecca, V. W., Herlyn, M., Smalley, K. S. M., & Anderson, A. R. A. (2011). Fibroblasts
499 contribute to melanoma tumor growth and drug resistance. *Molecular Pharmaceutics*, *8*(6),
500 2039–2049. doi: 10.1021/mp200421k
501 Flier, J. S., Underhill, L. H., & Dvorak, H. F. (1986). Tumors: Wounds That Do Not Heal. *New England*
502 *Journal of Medicine*, *315*(26), 1650–1659. doi: 10.1056/NEJM198612253152606
503 Fukumura, D., Xavier, R., Sugiura, T., Chen, Y., Park, E. C., Lu, N., Selig, M., Nielsen, G., Taksir, T.,
504 Jain, R. K., & Seed, B. (1998). Tumor induction of VEGF promoter activity in stromal cells.
505 *Cell*, *94*(6), 715–725. doi: 10.1016/s0092-8674(00)81731-6
506 Galiano, R. D., Michaels, V., Dobryansky, M., Levine, J. P., Gurtner, G. C., & others. (2004).
507 Quantitative and reproducible murine model of excisional wound healing. *Wound Repair and*
508 *Regeneration*, *12*(4), 485–492.
509 Glotzbach, J. P., Januszyk, M., Vial, I. N., Wong, V. W., Gelbard, A., Kalisky, T., Thangarajah, H.,
510 Longaker, M. T., Quake, S. R., Chu, G., & Gurtner, G. C. (2011). An Information Theoretic,
511 Microfluidic-Based Single Cell Analysis Permits Identification of Subpopulations among
512 Putatively Homogeneous Stem Cells. *PLOS One*, *6*(6), e21211. doi:
513 10.1371/journal.pone.0021211

514 Greenbaum, A., Hsu, Y.-M. S., Day, R. B., Schuettpelz, L. G., Christopher, M. J., Borgerding, J. N.,
515 Nagasawa, T., & Link, D. C. (2013). CXCL12 in early mesenchymal progenitors is required for
516 haematopoietic stem-cell maintenance. *Nature*, *495*(7440), 227–230. doi: 10.1038/nature11926
517 Hanahan, D., & Weinberg, R. A. (2011). Hallmarks of cancer: the next generation. *Cell*, *144*(5), 646–
518 674. doi: 10.1016/j.cell.2011.02.013
519 Helmlinger, G., Yuan, F., Dellian, M., & Jain, R. K. (1997). Interstitial pH and pO2 gradients in solid
520 tumors in vivo: high-resolution measurements reveal a lack of correlation. *Nature Medicine*,
521 *3*(2), 177–182. doi: 10.1038/nm0297-177
522 Hida, K., Akiyama, K., Ohga, N., Maishi, N., & Hida, Y. (2013). Tumour endothelial cells acquire drug
523 resistance in a tumour microenvironment. *Journal of Biochemistry*, *153*(3), 243–249. doi:
524 10.1093/jb/mvs152
525 Jaatinen, T., & Laine, J. (2007). Isolation of mononuclear cells from human cord blood by Ficoll-Paque
526 density gradient. *Current Protocols in Stem Cell Biology*, *Chapter 2*, Unit 2A.1. doi:
527 10.1002/9780470151808.sc02a01s1
528 Januszyk, M., Sorkin, M., Glotzbach, J. P., Vial, I. N., Maan, Z., Rennert, R. C., Duscher, D.,
529 Thangarajah, H., Longaker, M. T., Butte, A. J., & Gurtner, G. C. (2014). Diabetes Irreversibly
530 Depletes Bone Marrow-Derived Mesenchymal Progenitor Cell Subpopulations. *Diabetes*. doi:
531 10.2337/db13-1366
532 Kisanuki, Y. Y., Hammer, R. E., Miyazaki, J., Williams, S. C., Richardson, J. A., & Yanagisawa, M.
533 (2001). Tie2-Cre transgenic mice: a new model for endothelial cell-lineage analysis in vivo.
534 *Developmental Biology*, *230*(2), 230–242. doi: 10.1006/dbio.2000.0106

Lawrence, M. B., & Springer, T. A. (1991). Leukocytes roll on a selectin at physiologic flow rates: distinction from and prerequisite for adhesion through integrins. *Cell*, *65*(5), 859–873. doi: 10.1016/0092-8674(91)90393-d

Levi, B., Wan, D. C., Glotzbach, J. P., Hyun, J., Januszyk, M., Montoro, D., Sorkin, M., James, A. W., Nelson, E. R., Li, S., Quarto, N., Lee, M., Gurtner, G. C., & Longaker, M. T. (2011). CD105 protein depletion enhances human adipose-derived stromal cell osteogenesis through reduction of transforming growth factor β1 (TGF-β1) signaling. *The Journal of Biological Chemistry*, *286*(45), 39497–39509. doi: 10.1074/jbc.M111.256529

Li, G., Satyamoorthy, K., Meier, F., Berking, C., Bogenrieder, T., & Herlyn, M. (2003). Function and regulation of melanoma-stromal fibroblast interactions: when seeds meet soil. *Oncogene*, *22*(20), 3162–3171. doi: 10.1038/sj.onc.1206455

Mendt, M., & Cardier, J. E. (2017). Activation of the CXCR4 chemokine receptor enhances biological functions associated with B16 melanoma liver metastasis. *Melanoma Research*, *27*(4), 300–308. doi: 10.1097/CMR.0000000000000346

Möhle, R., Rafii, S., & Moore, M. A. (1998). The role of endothelium in the regulation of hematopoietic stem cell migration. *Stem Cells (Dayton, Ohio)*, *16 Suppl 1*, 159–165. doi: 10.1002/stem.5530160819

Nagasawa, T., Hirota, S., Tachibana, K., Takakura, N., Nishikawa, S., Kitamura, Y., Yoshida, N., Kikutani, H., & Kishimoto, T. (1996). Defects of B-cell lymphopoiesis and bone-marrow myelopoiesis in mice lacking the CXC chemokine PBSF/SDF-1. *Nature*, *382*(6592), 635–638. doi: 10.1038/382635a0

Newman, A. C., Nakatsu, M. N., Chou, W., Gershon, P. D., & Hughes, C. C. W. (2011). The requirement for fibroblasts in angiogenesis: fibroblast-derived matrix proteins are essential for

558 endothelial cell lumen formation. *Molecular Biology of the Cell*, *22*(20), 3791–3800. doi:
559 10.1091/mbc.E11-05-0393
560 Orimo, A., Gupta, P. B., Sgroi, D. C., Arenzana-Seisdedos, F., Delaunay, T., Naeem, R., Carey, V. J.,
561 Richardson, A. L., & Weinberg, R. A. (2005). Stromal fibroblasts present in invasive human
562 breast carcinomas promote tumor growth and angiogenesis through elevated SDF-1/CXCL12
563 secretion. *Cell*, *121*(3), 335–348. doi: 10.1016/j.cell.2005.02.034
564 Patten, R. D., Aronovitz, M. J., Deras-Mejia, L., Pandian, N. G., Hanak, G. G., Smith, J. J., Mendelsohn,
565 M. E., & Konstam, M. A. (1998). Ventricular remodeling in a mouse model of myocardial
566 infarction. *American Journal of Physiology-Heart and Circulatory Physiology*, *274*(5), H1812–
567 H1820. doi: 10.1152/ajpheart.1998.274.5.H1812
568 Schäfer, M., & Werner, S. (2008). Cancer as an overhealing wound: an old hypothesis revisited. *Nature*
569 *Reviews. Molecular Cell Biology*, *9*(8), 628–638. doi: 10.1038/nrm2455
570 Stratman, A. N., Malotte, K. M., Mahan, R. D., Davis, M. J., & Davis, G. E. (2009). Pericyte
571 recruitment during vasculogenic tube assembly stimulates endothelial basement membrane
572 matrix formation. *Blood*, *114*(24), 5091–5101. doi: 10.1182/blood-2009-05-222364
573 Suga, H., Rennert, R. C., Rodrigues, M., Sorkin, M., Glotzbach, J. P., Januszyk, M., Fujiwara, T.,
574 Longaker, M. T., & Gurtner, G. C. (2014). Tracking the Elusive Fibrocyte: Identification and
575 Characterization of Collagen-Producing Hematopoietic Lineage Cells During Murine Wound
576 Healing: Tracking Fibrocytes Without Surface Markers. *Stem Cells*, *32*(5), 1347–1360. doi:
577 10.1002/stem.1648
578 Tachibana, K., Hirota, S., Iizasa, H., Yoshida, H., Kawabata, K., Kataoka, Y., Kitamura, Y.,
579 Matsushima, K., Yoshida, N., Nishikawa, S., Kishimoto, T., & Nagasawa, T. (1998). The

chemokine receptor CXCR4 is essential for vascularization of the gastrointestinal tract. *Nature*, *393*(6685), 591–594. doi: 10.1038/31261

Teicher, B. A., & Fricker, S. P. (2010). CXCL12 (SDF-1)/CXCR4 pathway in cancer. *Clinical Cancer Research: An Official Journal of the American Association for Cancer Research*, *16*(11), 2927–2931. doi: 10.1158/1078-0432.CCR-09-2329

Ubil, E., Duan, J., Pillai, I. C. L., Rosa-Garrido, M., Wu, Y., Bargiacchi, F., Lu, Y., Stanbouly, S., Huang, J., Rojas, M., Vondriska, T. M., Stefani, E., & Deb, A. (2014). Mesenchymal-endothelial transition contributes to cardiac neovascularization. *Nature*, *514*(7524), 585–590. doi: 10.1038/nature13839

Valkenburg, K. C., de Groot, A. E., & Pienta, K. J. (2018). Targeting the tumour stroma to improve cancer therapy. *Nature Reviews. Clinical Oncology*, *15*(6), 366–381. doi: 10.1038/s41571-018-0007-1

Wagers, A. J., Sherwood, R. I., Christensen, J. L., & Weissman, I. L. (2002). Little evidence for developmental plasticity of adult hematopoietic stem cells. *Science (New York, N.Y.)*, *297*(5590), 2256–2259. doi: 10.1126/science.1074807

Wang, Y., Zheng, J., Han, Y., Zhang, Y., Su, L., Hu, D., & Fu, X. (2018). JAM-A knockdown accelerates the proliferation and migration of human keratinocytes, and improves wound healing in rats via FAK/Erk signaling. *Cell Death & Disease*, *9*(9), 848. doi: 10.1038/s41419-018-0941-y

Wong, V. W., Rustad, K. C., Galvez, M. G., Neofytou, E., Glotzbach, J. P., Januszyk, M., Major, M. R., Sorkin, M., Longaker, M. T., Rajadas, J., & others. (2010). Engineered pullulan–collagen composite dermal hydrogels improve early cutaneous wound healing. *Tissue Engineering Part A*, *17*(5–6), 631–644.

603 Zheng, B., Zhang, Z., Black, C. M., de Crombrugghe, B., & Denton, C. P. (2002). Ligand-dependent
604 genetic recombination in fibroblasts : a potentially powerful technique for investigating gene
605 function in fibrosis. *The American Journal of Pathology*, *160*(5), 1609–1617. doi:
606 10.1016/S0002-9440(10)61108-X

607